Multianode Photo Multiplier Tube Signal Response to Magnetic Fields up to 35 mT

R. Chamonal[1], S. Eisenhardt, F. Muheim
University of Edinburgh

Abstract

The performance of the 64-channel Multianode Photo Multiplier Tubes (MaPMT) has been studied with transverse and longitudinal magnetic fields up to 35 mT. The study shows that MaPMTs need shielding for fields greater than about 2.0 mT in order to limit the fraction of lost signals to the 10 percent or less. A 0.9 mm thick and 60 mm long μ-metal was successfully used to extend the operational range of use to at least ± 8.0 mT.

[1]Corresponding author: Email: chamonal@ph.ed.ac.uk

Contents

1 Introduction

For the optimised "LHCb light" detector the shielding plate in front of the LHCb dipole magnet was removed to allow for magnetic fields in the region between the VELO and the TT silicon tracker station. The bending of charged tracks in this region is exploited by the Level1 trigger. The fringe magnetic fields in the RICH 1 region have increased up to about 50 mT (500 G) where as the shielding plate had reduced the fringe fields to about 3 mT (30 G). Thus it became necessary to study the performance of the Multianode Photo Multiplier Tube (MaPMT) in higher magnetic fields. This study extends earlier measurements made up to magnetic fields of 3 mT. These have been included in Appendix A as only a summary of the results had been reported so far[2].

2 Experimental Settings

2.1 Apparatus

The setup used is shown in Figure 1. It consists of a magnet capable of producing an axial magnetic field up to 900 mT in a 12 cm wide gap. The current needed to produce a given magnetic field was calibrated with a Hall probe. The opening is wide enough to place the MaPMT tube, mounted in a separate housing, in any of the directions of the tubes coordinate system. The z-axis is the photo detector axis perpendicular to the photo cathode of the MaPMTs. Unless otherwise stated the measurements were taken with the MaPMT oriented in the z-direction, as the MaPMT is most sensitive to longitudinal magnetic fields, i.e. in the direction of the dynode structure.

Figure 1: *Magnet and MaPMT housing; corners: opened housing with the MaPMT and MaPMT coordinate system.*

A separate housing is designed to accommodate the readout and provide a light tight environment. As a light source we employ a ring of 4 blue LEDs with a wavelength of 430 nm, see the top corner plot of Figure 1. The end of the aluminum box is fitted with white paper which diffuses the light. This provides a sufficiently homogeneous light distribution at the MaPMT window.

The readout of the MaPMT is based on the APVm chip and is basically the same as described in [1]. Only minor modifications were made to adapt for the space constraints here. Two MaPMTs with slightly different properties were tested. These differ by the geometry of the focusing wires and the entry windows. See reference [1] for further details. The two tubes are referred to in the text by their serial numbers: 9C24C1 for the old and 9K20C3 for the new type, respectively.

2.2   Data Acquisition

The high voltage of the MaPMT was set to -1000 V. The trigger rate was chosen to be 1 kHz and exactly 24558 events were taken per run. The magnetic field was varied in the range from 0 mT to ±35 mT: in steps of 1 mT up to ±10 mT and in steps of 5 mT thereafter. The procedure was as follows: First a pedestal run was taken for which the LEDs were switched off. Then a measurement at 0 mT was taken with the amount of light adjusted to a level where for each individual MaPMT channel in 20 ... 30 % of the events a signal occurred. The sequence of measurements then followed a hysteresis curve: first a series of data were taken by increasing the negative magnetic field from zero to its maximum value and decreasing it back to zero (15 values per direction). After switching the polarity of the magnet power supply another pedestal run was taken and the procedure was repeated for positive magnetic fields. It turned out that the hysteresis of the magnet could be neglected for this range of fields.
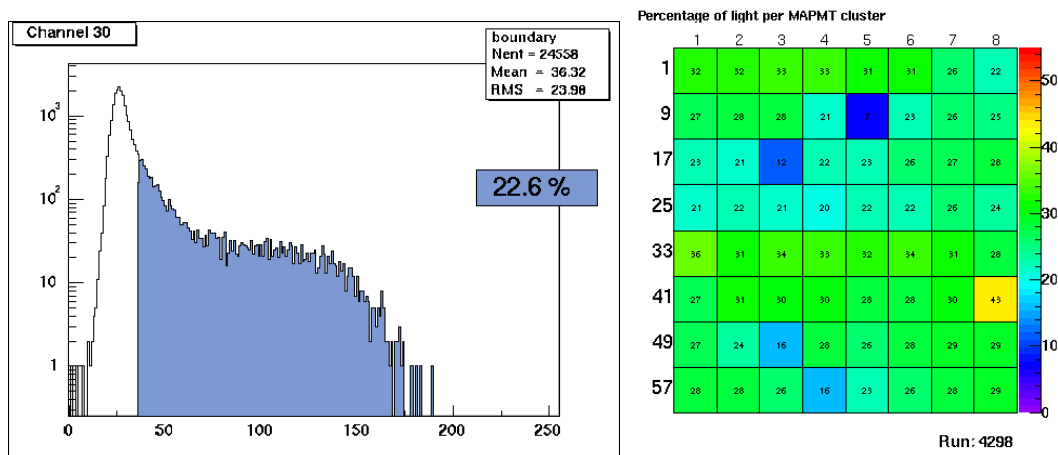

Figure 2: *Left: the spectrum of channel 30 with the signal fraction shaded; Right: the signal fractions (in percentages) measured for the 8x8 channels of a MaPMT.*

2.3   Data Analysis

The produced raw data were transferred to and analysed on a Linux based system. First, each run undergoes an event-by-event common mode correction based on the latest pedestal

run. Afterwards, for each channel a Gaussian fit was applied around the pedestal region. Using the fit results for the pedestal position, Q_0, and width, σ, a threshold value $Q_0 + 5 * \sigma$ was defined for each channel. All entries above the threshold cut were regarded as signal from a photoelectron. The signal fraction, the ratio of signals to all events, was tuned to be within $20 \ldots 30\,\%$ for the average of the 64 channels of a tube for a zero external field. Figure 2 shows the signal spectrum of a single channel at $0\,\mathrm{mT}$ with the signal area shaded. It also shows a map of a MaPMT indicating the signal fraction (in percentages) measured for the 64 channels.

Channels with problems were masked and not used for the analysis. This was always true for channel 48 which had a problem in the front-end electronic resulting in a double pedestal peak. But also channels which suffered from low gain (channels 13, 19, 51, 60 in Figure 2) were excluded.

3   Signal Response to Magnetic Field

3.1   Global Signal Fraction

The global signal fraction of the MaPMT is defined as the average over the individual signal fractions of all channels of a MaPMT, i.e. the sum over all signal entries of a tube normalised by the number of events and the number of channels. To study the behaviour in the magnetic field the result then is normalised to the value found for zero external field. In Figure 3 the results are displayed for magnetic fields in the longitudinal (tube 9K20C3) and transverse direction (tube 9C24C1). In the case of a longitudinal field the
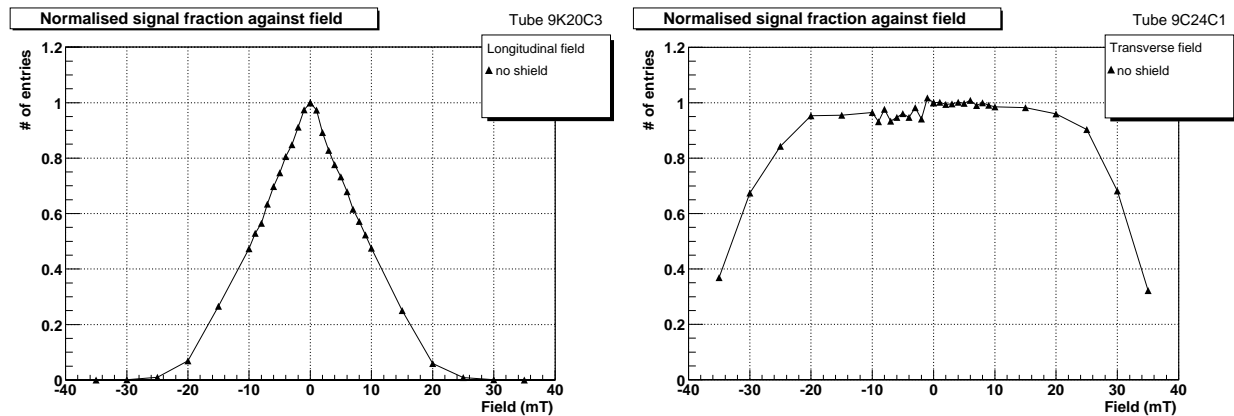

Figure 3: *The global signal fraction of a MaPMT as a function of the magnetic field. Left: field in longitudinal z-direction; Right: field in transverse x-direction.*

signal fraction starts to decrease as soon as a field is applied. The decrease is to a good approximation proportional to the shield strength, and it is slightly stronger for positive fields up to $10\,\mathrm{mT}$. If the tube is not shielded the signal fraction drops to $90\,\%$ around $2\,\mathrm{mT}$ and to $80\,\%$ between 3.5 mT to $4.0\,\mathrm{mT}$, respectively. In the case of transverse fields only the x-direction has been tested. From previous tests it was known that the y-direction does not behave significantly different. The results show that the MaPMT is quite insensitive to transverse magnetic fields in the range up to $\pm 20\,\mathrm{mT}$ where the global or average signal
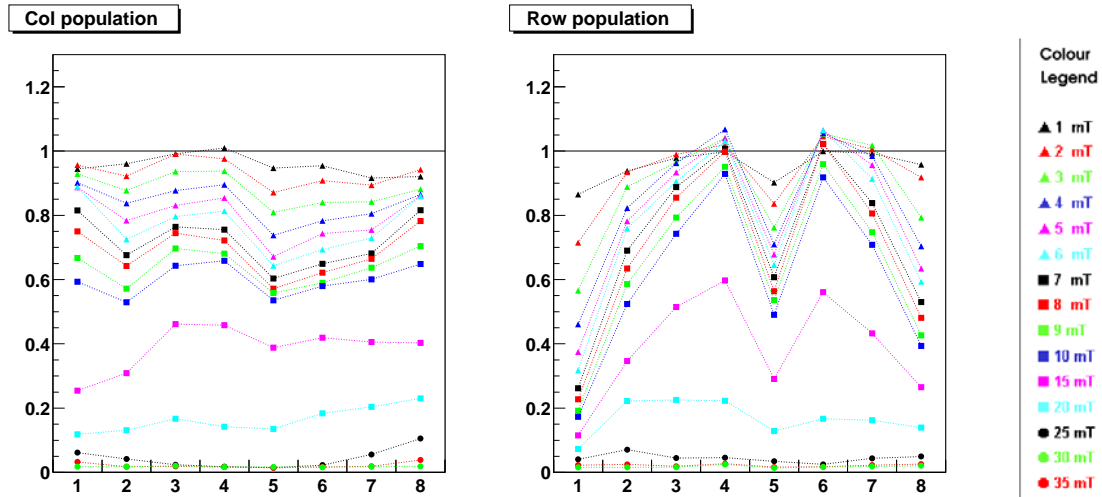
Figure 4: *Normalised signal fraction for columns and rows versus column and row number, respectively. Points taken at the same field are joined by a dashed line to guide the eye.*

fraction decreases only by less than 10 %. At higher field the signal fraction starts to drop sharply, finally with a rate comparable to the case of longitudinal fields.

3.2 Signal Fraction on Groups of Rows and Columns

To learn about the pattern of signal response in different regions of the MaPMT the signal fraction has been studied in rows and columns of channels. A row of a MaPMT is defined by eight adjacent channels in the horizontal or x-axis, using the Hamamatsu labelling (see channel map in Figure 2). For example, row 2 is formed by channels 9 to 16. A column is defined by eight adjacent channels in the vertical or y-axis, e.g. column 2 is defined by channels 2, 10, ... 58. The signal fraction is averaged over the channels of a row or column, respectively, and then normalised to the measurements without field.

Results for longitudinal negative fields are displayed in Figure 4. To guide the eye the measurements for eight columns or rows taken with the same magnetic field are connected by lines. In the case of columns a progressive loss of the signal fraction is found which is approximately proportional to the field strength until virtually no signal is measured anymore at 25 mT. The behaviour is very similar for all columns, and it matches the dependence of the global (average) signal fraction plotted in Figure 3.

For the rows a different behaviour for the signal fraction versus magnetic field is observed. The rows on top and the bottom of the tube exhibit a decrease of the signal fraction which is much stronger than for the rows in the center of the tube. This rapid loss of signal in the top and bottom rows of the MaPMT is genuine to the tube (see Section 4.1). This behaviour is the same for negative and positive fields and the old and new types of the MaPMT. A strong decrease is also visible in row 5. This decrease is due to a large electronic cross-talk with row 1 (see Section 4.2 for more details). Without this cross-talk row 5 behaves like its neighbours.

To better illustrate these results, we also plot the normalised signal fraction versus the applied magnetic field for selected rows of pixels for tube 9C20A2, see Figure 5. We measure that the signal fraction of row 3 (squares) decreases by less than 10% up to longitudinal
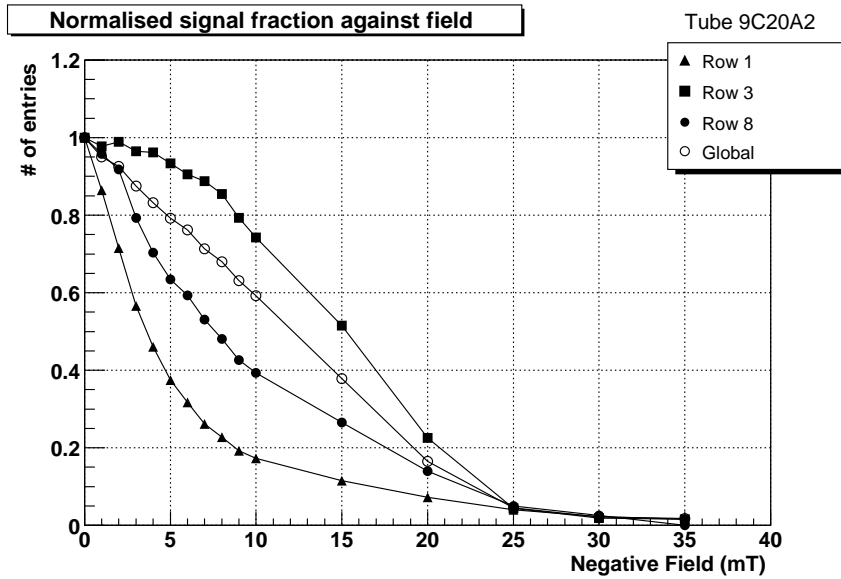
Figure 5: *Normalised signal fraction for columns versus the longitudinal negative magnetic field for rows 1, 3, 8 and for the global average.*

fields of 5 mT (50 G). A very similar behaviour is observed for all other centre rows (2 to 7). We conclude that three quarters of the MaPMT channels are rather insensitive to longitudinal fields up to 5 mT (50 G). However, the top (triangles) and bottom (filled bullets) rows lose up to 50% of the signal already at 3 mT (30 G). We observe that the top and bottom rows of the MaPMT are sensitive to fields above 1 mT (10 G). Also shown is the averaged global signal fraction (open bullets) which stays above 90% up to fields of about 2 mT (20 G).
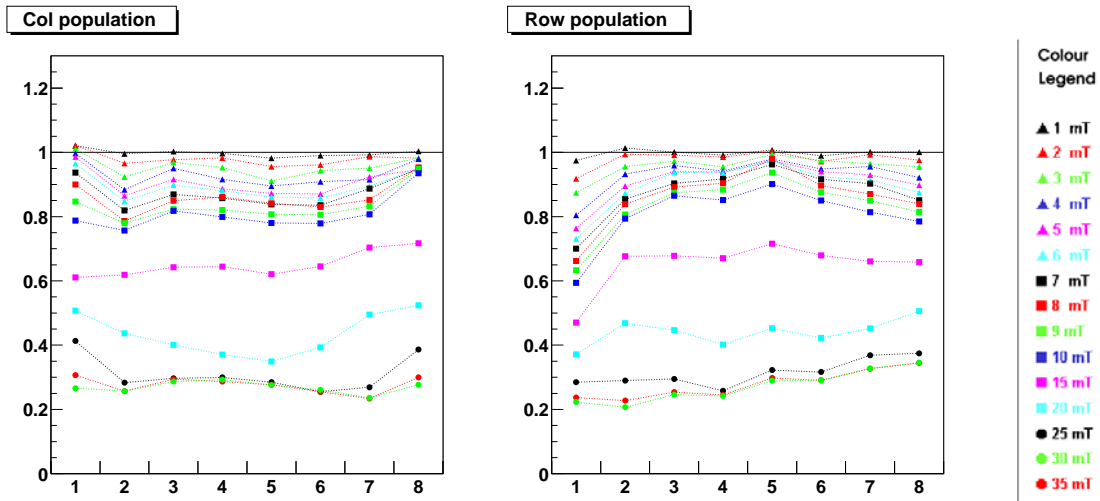

Figure 6: *Center of Gravity of signal hits for columns and rows versus column and row number, respectively. Points taken at the same field are joined by a dashed line to guide the eye.*

4 Nature of the Losses

4.1 General Case

In order to find out the nature of the loss in the MaPMT, the gain of the tube has been estimated by calculating the center of gravity (COG), i.e. the first momentum of the signal, for each channel of all measurements. The average of all COGs is calculated for the channels of a row or column, respectively. Again the result is normalised using the measurement at zero external field as reference. The results are displayed in Figure 6. It shows that the COG decreases significantly less than the signal fraction displayed in Figure 4. The average loss of gain is less than 10% for longitudinal fields up to 5 mT. This suggests that the decline of the signal fraction with increased magnetic field predominantly has to be attributed to primary photoelectrons being lost before the entry to the dynode structure. A smaller fraction of the signal is lost due to a reduction in gain, i.e. electrons lost within the dynode structure.

4.2 Case of Row 5

The signals in row 5 are subject to a strong asymmetric, i.e. one-way, cross talk from signals of row 1. This is part of the cross talk behaviour identified in the APVm readout in [2] and is attributed to cross talk internal to the APVm chip. The effect of the cross talk was verified by the application of a pinhole mask in front of the MaPMT which covered all but the channels of row 1. The result of this measurement is illustrated in Figure 7. It clearly shows a cross talk in excess of 50 % from the channels of row 1 to row 5. In the other direction no significant cross talk is observed, see Figure 8. That means that a loss of signal in row 1 will show up in row 5 like seen in Figure 4. If only row 5 is illuminated the signal fraction drops in a similar way as the other center rows of the tube.

Figure 7: *Cross-talk between row 1 and row 5.*

5 Transverse Spill-Over

The spill-over of signal into neighbouring channels due to an external field was studied as well. A pinhole mask was placed in front of the MaPMT leaving only the pixels in row 5 exposed to LED light. Then the signal fraction of the channels adjacent to the top and bottom of an illuminated channel was regarded. It was normalised by the signal fraction of the illuminated channel and displayed as a function of the magnetic field in longitudinal and transverse direction. An increase of this ratio to one side of the illuminated channel would indicate a spill-over of signal to the neighbour. This could happen by photoelectrons emitted from the cathode being diverted to the entry window of the neighbouring channel or by the distortion of the electron trajectories between the dynodes resulting in a charge sharing of the two adjacent channels.
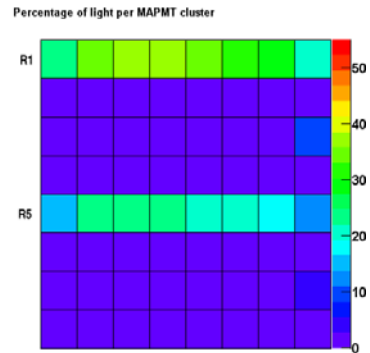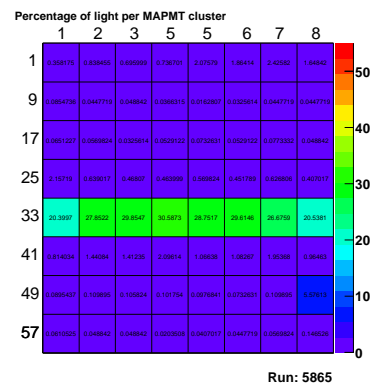

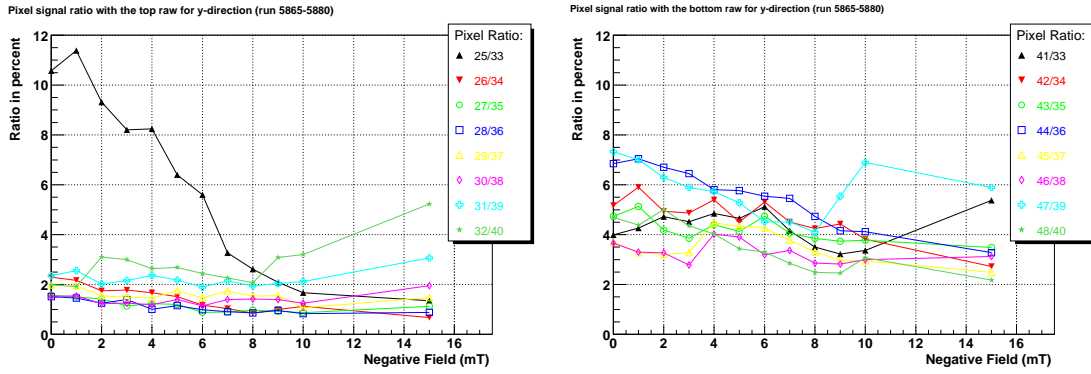Figure 8: *Only row 5 illuminated.*

8

Figure 9: *Signal spill-over for longitudinal fields for channels adjacent to row 5 (of tube 9K20C3); Left: channels of row 4, Right: channels of row 6; lines connect the results for each pixel to guide the eye.*
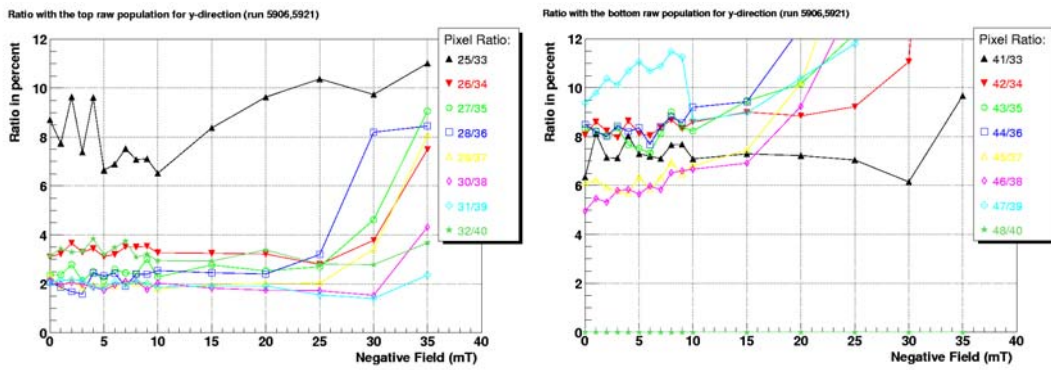

Figure 10: *Signal spill-over for transverse fields for channels adjacent to row 5 (of tube 9K20C3); Left: channels of row 4, Right: channels of row 6; lines connect the results for each pixel to guide the eye.)*

5.1 Longitudinal Field

Figure 9 presents the results for longitudinal fields where the results for each pixel are connected by a line to guide the eye. At least up to 10 mT the ratio of signal fractions stays stable, i.e. no signal spill-over is found.

Beyond 15 mT the absolute number of signals in the spectra becomes so low that the statistical error becomes to big to draw a conclusion in that region. Only the behaviour of channel 25 differs from the other channels for which no explanation can be given, but it is likely that the pinhole was not centered well on this pixel.

5.2 Transverse Field

Figure 10 presents the results for transverse fields where again the results for each pixel are connected by a line to guide the eye. In this case the region of a stable ratio of the signal fractions extends up to 25 ... 30 mT for the upper row or 15 ... 20 mT for the lower row. This is consistent with the extended region of small signal loss for the transverse fields as shown in Figure 3. In conclusion again no sign of a signal spill-over is seen for the region where the measurement is not dominated by small signal fractions and thus large

statistical fluctuations.

As for the case of longitudinal fields the behaviour for channel 25 is different that for the other channels.

6 Effect of Shielding

The loss of photoelectrons due to a magnetic field has to be minimised for the application of MaPMTs as photodetectors of the LHCb RICH detectors. Thus, with respect to the case of zero field an efficiency of $90\,\%$ is required for the recognition of a signal above the threshold cut. As demonstrated with Figures 3 and 5 this limit is already reached with a longitudinal field of about $2\ldots 3\,$mT. To extend the working range of the MaPMT in external magnetic fields measurements were performed with a prototype of an individual μ-metal shield.

The conclusion of Section 4.1 confirms the expectation that the MaPMT is most sensitive to magnetic fields in the region between the photo cathode and the first dynode. Therefore the strength of shielding in this region dominates the overall effect of the shields.

6.1 The μ-metal Shield Prototype

The prototype for the individual μ-metal shielding of the MaPMTs consisted of a square tube of $60\,$mm length with a wall thickness of $0.9\,$mm. The inner and outer diameter of the shield were $29.5 \pm 0.3\,$mm and $31.5 \pm 0.3\,$mm, respectively. The shield was placed around the MaPMT and the base as illustrated in Figure 11. To test whether the single shield would possibly start to saturate measurements were carried out with a second shield placed around the first. The second shield had inner and outer diameters of $32.5 \pm 0.3\,$mm and $34.5 \pm 0.3\,$mm, respectively.

Two positions of the photocathode within the shield were chosen. With the photocathode recessed by $20\,$mm with respect to the end of the shield, the MaPMT was centrally placed within the shield. The measurements taken with a recess of only $13\,$mm were directly comparable with the measurements taken earlier (see Appendix A) and resembled a solution more preferred for a final system for mechanical reasons. Note that in a final system the single base will be replaced by a bleeder board serving several MaPMTs so that the individual shields around the MaPMTs have to end at the rear side of the MaPMT.
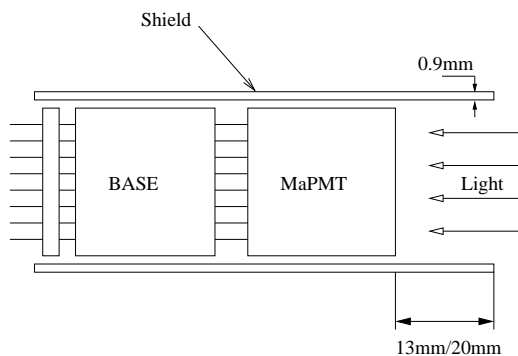

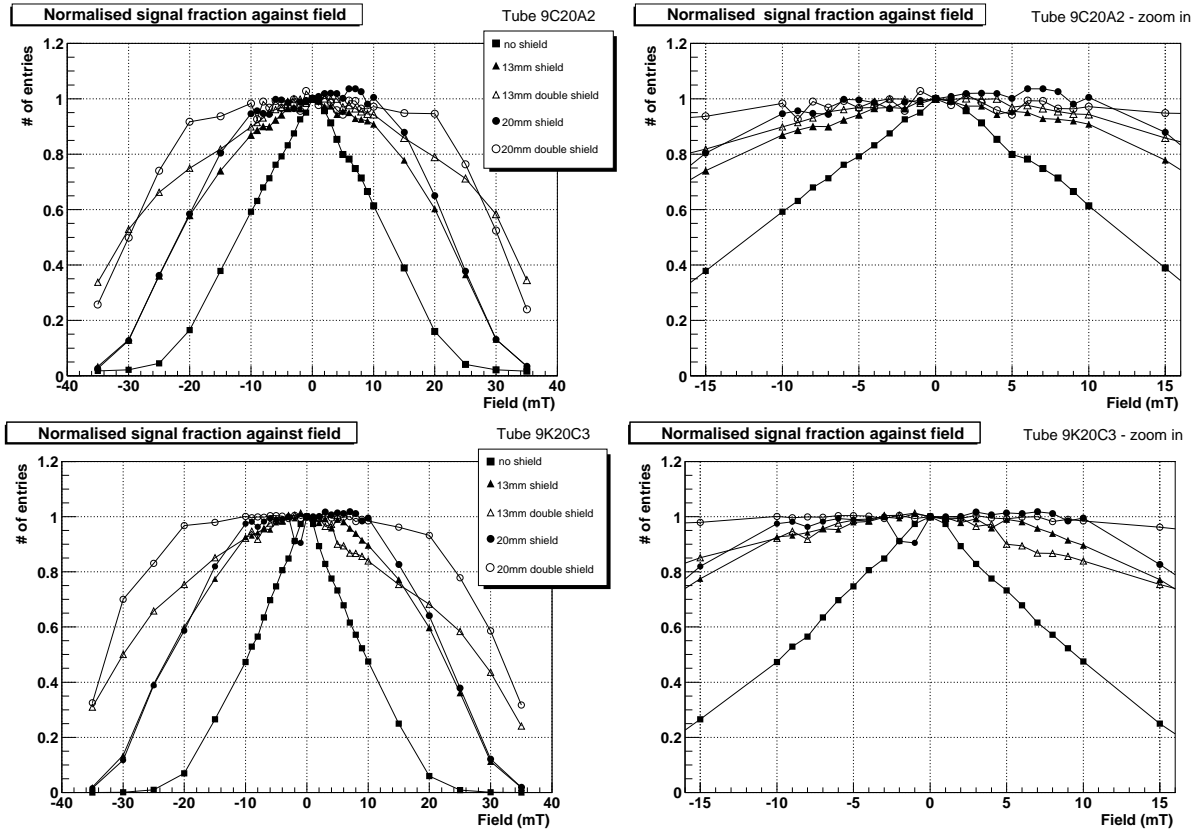Figure 11: *The μ-metal shield around the MaPMT and base.*

Figure 12: *Normalised signal fraction for tube 9C20A2 (top) and the tube 9K20C3 (bottom) with and without shielding as a function of the magnetic field, for the full range (left) and zoomed into the $\pm 15\,mT$ range (right).*

6.2   Results

Measurements have been made for the old (9C20A2) as well as the new (9K20C3) type of MaPMT as the two types differ exactly in the region where they are most sensitive to magnetic fields. Data were taken for the most critical case of longitudinal magnetic fields. The results are summarised in Figure 12. Plotted are the measurements for the case of an unshielded MaPMT as a reference, for the case of the application of a single shield and finally for the additional application of a second shield.

As discussed for Figure 3, in the unshielded case the signal fraction decreases linearly with an external field applied. The MaPMT with the new focusing layout (9K20C3) is slightly more sensitive than the old type (9C20A2), e.g. at $\pm 10\,\mathrm{mT}$ the signal fraction for the old and new type is reduced to $\approx 60\,\%$ and $\approx 50\,\%$, respecively, but as only two tubes were measured the difference is too small to state that the new type is more sensitive to longitudinal magnetic fields. The difference in sensitivity also vanishes when an individual μ-metal shield is applied. In both cases, a signal fraction of $\approx 60\,\%$ is found for field of $\pm 20\,\mathrm{mT}$ and the behaviour up to $\pm 10\,\mathrm{mT}$ is similar. For the case of a 13 mm recess, the limit of a 10 % drop in the signal fraction is reached at about $\pm 8\,\mathrm{mT}$. For the case of a 20 mm recess this limit is reached beyond $\pm 10\,\mathrm{mT}$. At $\pm 10\,\mathrm{mT}$ the signal fraction rather drops by about 5 %.

By applying a second sheath of μ-metal one increases the magnetic flux which can be

drawn away from the position of the MaPMT and thus extend the range of fields under which it can be operated. As the second shield has a larger diameter it should be less efficient than the first shield. This is visible in Figure 12. No significant difference is found in the range ± 10 mT where the first sheath already provides efficient shielding. Beyond that the second sheath improves the total shielding power but it does not double the range for which a certain level of signal fraction can be achieved.

In the interesting region of fields within ± 10 mT the positive effect of a recess of 20 mm in comparison with a recess of 13 mm is much more favourable than the addition of extra shielding material. Only if the environment provides fields beyond ± 10 mT thicker shields have to be incorporated to the design of the RICH photodetectors.

7 Summary and Conclusions

The signal response of MaPMTs has been studied in magnetic fields up to 35 mT (350 G). We observe that the MaPMTs are most sensitive to external fields perpendicular to the entry window, i.e. along the longitudinal axis. Compared to that the sensitivity to fields along the perpendicular axes is small. The loss of signal fraction is below 10 % for fields up to 20 mT (200 G) and can be neglected. The loss of signal is predominantly due to electrons lost between the photocathode and the entry window of the dynode structure. Compared to that a smaller fraction is lost due to a reduction in signal gain, i.e. electrons lost further down the dynode chain. The signal loss is not uniform over the sensitive area of the tube. The most affected channels are the top and the bottom rows of the tube (Hamamatsu channel labelling). No signs were found for spill-over induced by the magnetic field, i.e. that a signal spills over into an adjacent channel due to the magnetic field.

By requiring a maximum average signal loss of 10 % we determined that MaPMTs need shielding for longitudinal fields equal or larger than 2.0 mT (20 G). However, the centre rows are quite insensitive to fields up to 5.0 mT (50 G) and most of the losses are in the top and bottom rows which are already sensitive to fields 1.0 mT (10 G). Efficient shielding of the MaPMT can be provided with a 0.9 mm individual μ-metal shield and the operational range of the tubes can be extended to higher fields. With a recess of the MaPMT window of 13 mm the average signal loss stays below 10 % up to about ± 8 mT. With a recess of 20 mm the operational range can be extended even more to about ± 12 mT, and the signal loss is significantly reduced compared to the case of a 13 mm recess. If the MaPMTs needs to be operated in an environment beyond ± 10 mT additional μ-metal should be foreseen to draw away more of the magnetic flux, e.g. twice the wall thickness for fields up to about ± 20 mT.

References

[1] S. Eisenhardt *et al.*, "Performance of Multianode Photo Multiplier Tubes at Low Gain"; LHCb 2003-043 RICH, June 2003.

[2] E. Albrecht *et al.*, "Performance of a cluster of multi-anode photomultipliers equipped with lenses for use in a prototype RICH detector",
Nucl. Instrum. Meth. A **488**, 110-130 (2002).

8   Appendix A

In the following we describe measurements which were carried out before the RICH Technical Design Report. At this time, the strength of the fringe magnetic fields due to the LHCb dipole magnet were expected to be up to 30 G in the vicinity of the RICH photodetectors. Only a summary of these results has been published[2]. Here we report details of these measurements.
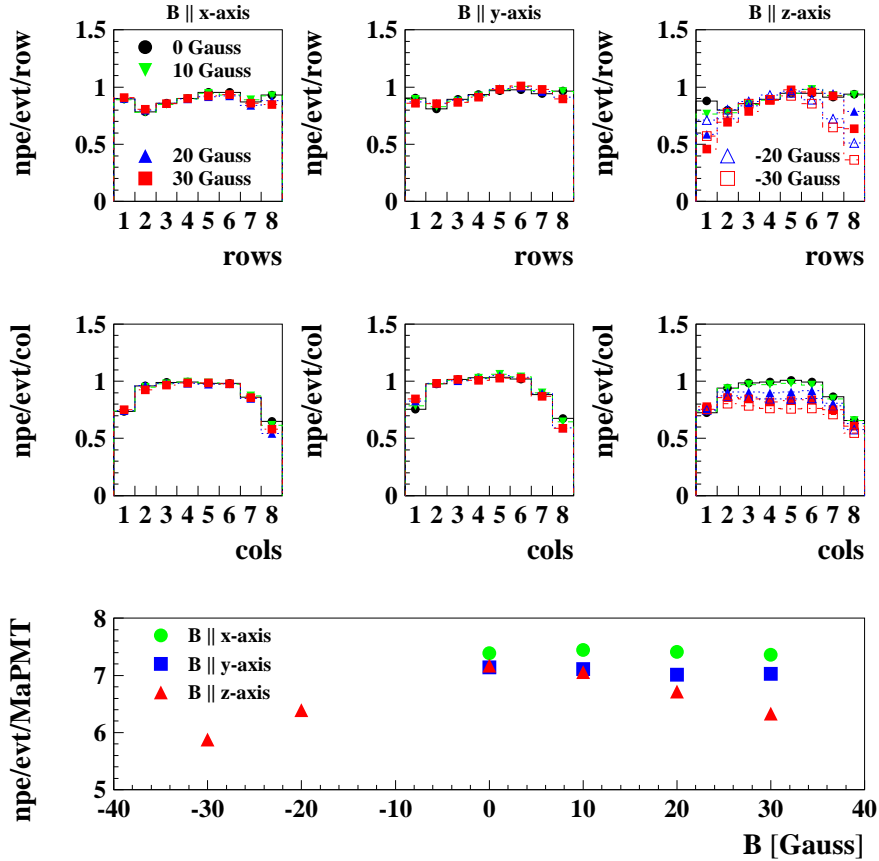

Figure 13: *Number of photo electrons n_{pe} measured in an unshielded MaPMT for B fields up to 30 G and for different field orientations. Top and Middle: n_{pe} measured in a row (column) versus row (column) number. Bottom: n_{pe} in the MaPMT as a function of B.*

The sensitivity of the MaPMT to a magnetic field has been studied by placing a single tube within a Helmholtz coil providing an axial magnetic field up to 3 mT (30 G). Using an LED light source, the relative efficiency of a tube has been measured for magnetic fields transverse (B_x and B_y) and longitudinal (B_z) to the photodetector axis. In the top and middle rows of Figure 13 we show the measured number of photoelectrons n_{pe} in a row (column) of pixels versus the row (column) number for magnetic fields up to 30 G in the three field orientations. The measured n_{pe} summed over all 64 MaPMT pixels as a function of the B_z is plotted in the bottom picture of Figure 13. These results demonstrate that the MaPMT has little sensitivity to transverse magnetic fields up to 30 G. For longitudinal

fields of $B_z \geq 10$ G the efficiency of the MaPMT deteriorates. This loss occurs mostly in the two edge rows parallel to the x-axis where the focusing of the photoelectrons onto the first dynode is most sensitive to magnetic fields. At $B_z = 30$ G the collection efficiency of the edge rows is reduced to about 50% with respect to that at $B_z = 0$ G.
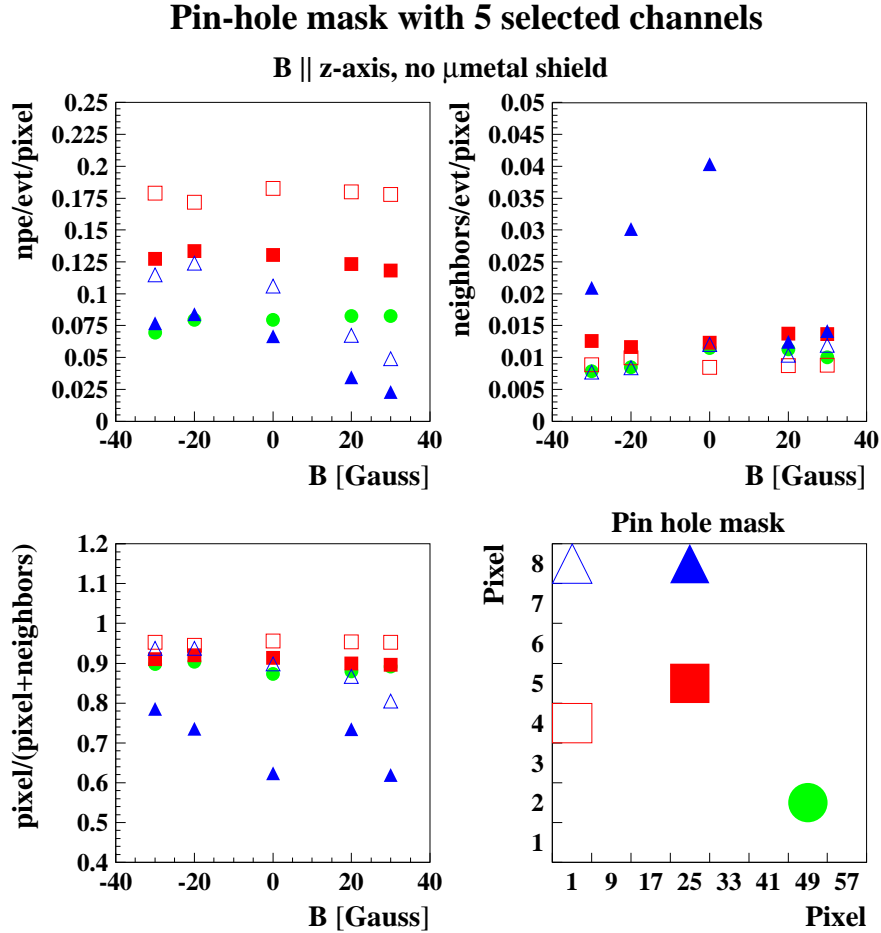
Pin-hole mask with 5 selected channels

B || z-axis, no μmetal shield

Figure 14: *Measured yield of photo electrons versus B_z for selected pixels of an MaPMT. Top Left: n_{pe} in selected pixels. Top Right: n_{pe} in neighbors of selected pixels. Bottom left: fraction of signal in selected pixel versus selected pixel including neighbors. Bottom right: the five selected pixels and their labels.*

Additional measurements have been carried out with a pin-hole mask in front of the MaPMT window to better define the aperture of the individual pixels. No significant differences with respect to the data recorded without a mask have been observed. The effect of the magnetic fields on selected pixels has also been investigated. These results are plotted in Figure 14: the five selected pixels and their labels are shown in the bottom right picture. In the top left and top right plot we show the measured number of photo electrons as a function of the longitudinal magnetic field for the selected pixels and in their nearest neighbours, respectively. The fraction of signal in the pixel itself is plotted in the bottom left picture. For the two top row pixels (open and filled blue triangles), the decrease of signal with increasing magnetic field is clearly visible. The fraction of light recorded on the neighboring pixels does not depend on the magnetic field and we do not observed photo

14

electrons crossing over to neighbouring dynode chains. The fluctuations for pixel 32 (blue triangles) are not understood, but the mask was likely not centered well on this pixel.
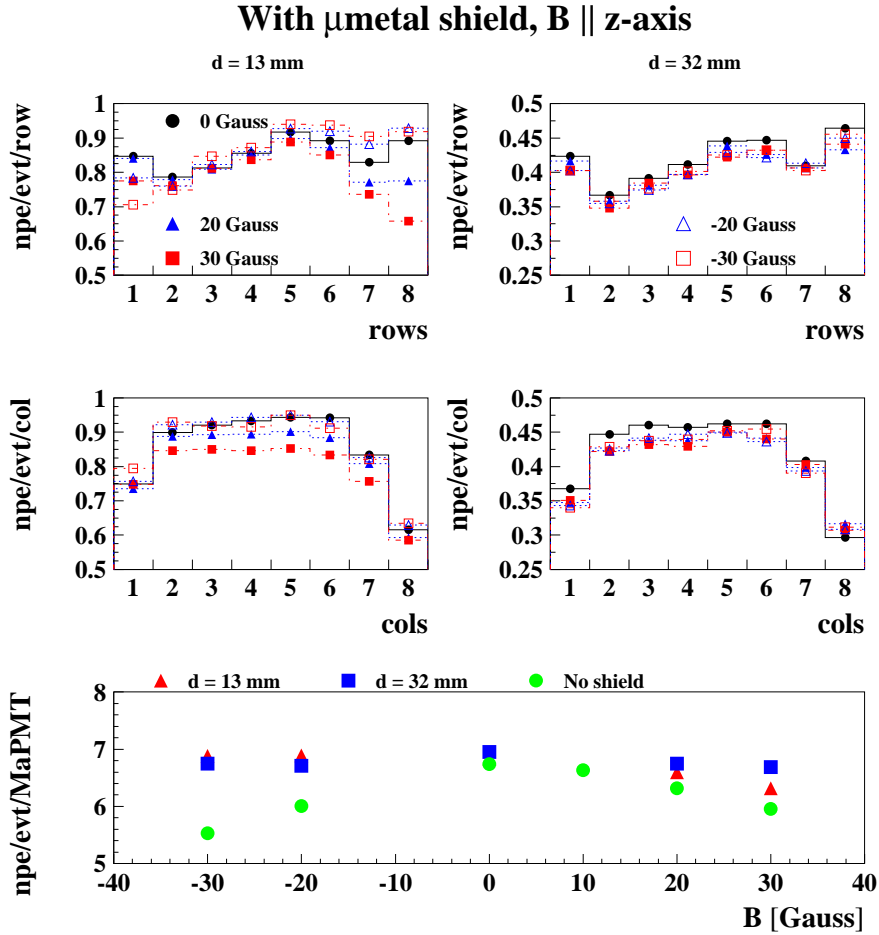
With μmetal shield, B ∥ z-axis

Figure 15: *The number of observed photo electrons n_{pe} for an MaPMT shielded with a μ-metal tube extending for two different lengths d (see text) beyond the entry window. Top and Middle: n_{pe} measured in a row (column) versus row (column) number for different B_z. Bottom: n_{pe} in the MaPMT as a function of B_z.*

We also studied the effect of shielding the MaPMT with a μ-metal tube of square cross–section with a width 30 mm, length 60 mm and wall thickness 0.9 mm. The shield enclosed the tube and extended beyond the MaPMT window face by a distance d. In Figure 15 top and middle, we show the measured number of photoelectrons in a row (column) of pixels versus the row (column) number for two values of d (13 mm and 32 mm). The measured number of photoelectrons in all pixels of the MaPMT as a function of B_z without and with the shield, for two values of d (13 mm and 32 mm) is shown in Figure 15 bottom). The μ-metal tube is effective in reducing the efficiency loss; with an extension of 32 mm or more there is no detectable loss in efficiency due to the 30 G field. We conclude that the MaPMT can be effectively shielded with a μ-metal structure up to fields of 30 G.